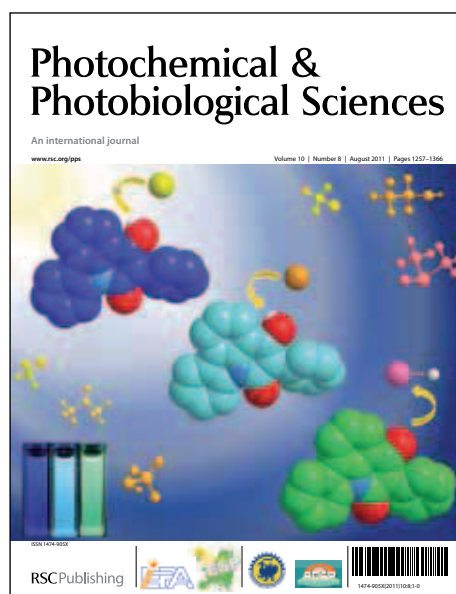


Photochemical & Photobiological Sciences

Accepted Manuscript



This is an *Accepted Manuscript*, which has been through the RSC Publishing peer review process and has been accepted for publication.

Accepted Manuscripts are published online shortly after acceptance, which is prior to technical editing, formatting and proof reading. This free service from RSC Publishing allows authors to make their results available to the community, in citable form, before publication of the edited article. This *Accepted Manuscript* will be replaced by the edited and formatted *Advance Article* as soon as this is available.

To cite this manuscript please use its permanent Digital Object Identifier (DOI®), which is identical for all formats of publication.

More information about *Accepted Manuscripts* can be found in the [Information for Authors](#).

Please note that technical editing may introduce minor changes to the text and/or graphics contained in the manuscript submitted by the author(s) which may alter content, and that the standard [Terms & Conditions](#) and the [ethical guidelines](#) that apply to the journal are still applicable. In no event shall the RSC be held responsible for any errors or omissions in these *Accepted Manuscript* manuscripts or any consequences arising from the use of any information contained in them.

Synthesis of some fluorescent benzimidazole derivatives using cobalt(II) hydroxide as high efficient catalyst - Spectral, physico-chemical studies and ESIPT process

J. Jayabharathi^{*}, V. Thanikachalam, K. Jayamoorthy

Department of Chemistry, Annamalai University, Annamalainagar 608 002, Tamilnadu, India.

* Address for correspondence

Dr. J. Jayabharathi
Professor of Chemistry
Department of Chemistry
Annamalai University
Annamalainagar 608 002
Tamilnadu, India.
Tel: +91 9443940735
E-mail: jtchalam2005@yahoo.co.in

* Corresponding author Tel.: +91 9443940735
E-mail address: jtchalam2005@yahoo.co.in

Synthesis of some fluorescent benzimidazole derivatives using cobalt(II) hydroxide as high efficient catalyst - Spectral, physico-chemical studies and ESIPT process

J. Jayabharathi^{*}, V. Thanikachalam, K. Jayamoorthy

Department of Chemistry, Annamalai University, Annamalainagar 608 002, Tamilnadu, India.

Abstract

Some fluorescent benzimidazole derivatives have been designed and synthesized using cobalt(II) hydroxide as high efficient catalyst. Synthesized compounds have been characterized by ^1H , ^{13}C -NMR and mass spectral analysis. The solvent effect on the absorption and fluorescence bands has been analyzed and supplement by computational studies. Solvatochromic effects on the spectral position and profile of the stationary fluorescence spectra clearly indicate the charge transfer (CT) character of the emitting singlet states of all of the compounds studied both in a polar and a non polar environment. The fluorescence decays for the benzimidazoles fit satisfactorily to a single exponential kinetics. HOMO and LUMO orbital picture [DFT/B3LYP/6-31G(d,p)] evidence the existence of excited state intramolecular proton transfer (ESIPT) in benzimidazole derivative containing hydroxy group.

Keywords: benzimidazole; cobalt(II) hydroxide; DFT; ESIPT; HOMO-LUMO; CT.

^{*} Corresponding author. Tel.: +91 9443940735
E-mail address: jtchalam2005@yahoo.co.in

1. Introduction

Benzimidazole based chromophore have received increasing attention due to their distinctive linear, non-linear optical properties and also due to their excellent thermal stability in guest-host systems [1]. Hydrogen bond plays an important role as a site specific interaction in most of the acid–base chemical and biological systems. The electrostatic interactions such as N–H...N, N–H...O, O–H...N, O–H...O [2, 3], and other similar interactions between neutral H and O, N, etc. with bond length ranging from 1.5 to 2.4 Å [4] have been studied. Excited state intramolecular proton transfer (ESIPT) has become a field of active research [5, 6] due to the practical applications of ESIPT exhibited by molecules as laser dyes [7], photostabilizers [8], fluorescent probes in biology [9] and light-emitting materials for electroluminescent devices [10]. Phototautomerisation through ESIPT is of prime importance in biological and chemical systems leading to experimental and theoretical interests [11-15]. Photophysical studies on bioactive molecules with phenolic function are of our interest; they exhibit ESIPT.

The electronic transition in molecules, involving intramolecular charge transfer (ICT), is very sensitive to the nature of the microenvironment around the solute and the spectral parameters can be used for studying solute-solvent interaction at the microscopic level [16]. The CT character of fluorescent state of the biaryl molecules in polar solvents seems to be well proved by the large Stokes shift, the large dipole moment change upon excitation and by the time-resolved fluorescence [17-20] and transient absorption studies [21]. In this article, we report the elegant catalytic synthesis, characterisation and solvatochromism of benzimidazole molecules with fluoro-, methyl-, methoxy-, trifluoromethyl-, hydroxy- and substituents along with the unsubstituted one. The solvent-dependent photophysical characteristics of benzimidazole derivatives were investigated by steady-state absorption and emission spectroscopy as well as time resolved fluorometry. From these experiments, we

determined the position of the spectral maxima (λ_{abs} , λ_{ex} and λ_{emi}), the Stokes and lifetime (τ), and the rate constants of radiative (k_r) and nonradiative (k_{nr}) deactivation of benzimidazole derivatives. We used the Lippert solvent parameter Δf , the normalised $E_T(30)$ polarity scale, and the multiparameter Kamlet-Taft and Catalan solvent scales to describe the solvent effect on the fluorescence emission maxima and Stokes shift of benzimidazole derivatives. We have also addressed the influence of solvents on the photophysical properties of the synthesized molecules in terms of $hc\tilde{\nu}_{\text{abs}}^{\text{vac}}$, $hc\tilde{\nu}_{\text{flu}}^{\text{vac}}$ and $(hc\tilde{\nu}_{\text{abs}}^{\text{vac}} - hc\tilde{\nu}_{\text{flu}}^{\text{vac}})$ with solvent polarity function. Single crystal X-ray diffraction (XRD) analysis and density functional theory (DFT) calculations support the ESIPT in hydroxy benzimidazole derivative.

2. Experimental

2.1. Spectral measurements

The proton spectra at 400 MHz were obtained at room temperature using a Bruker 400 MHz NMR spectrometer. Proton decoupled ^{13}C NMR spectra were also recorded at room temperature employing a Bruker 400 MHz NMR spectrometer operating at 100 MHz. The mass spectra of the samples were obtained using a Thermo Fischer LC-Mass spectrometer in fast atom bombardment (FAB) mode. The UV-vis absorption and fluorescence spectra were recorded with PerkinElmer Lambda 35 spectrophotometer and PerkinElmer LS55 spectrofluorimeter, respectively. Fluorescence lifetime measurements were carried out with a nanosecond time correlated single photon counting (TCSPC) spectrometer Horiba Fluorocube-01-NL lifetime system with NanoLED (pulsed diode excitation source) as the excitation source and TBX-PS as detector. The slit width was 8 nm and the laser excitation wavelength was 280 nm. The fluorescence decay was analyzed using DAS6 software. The photoluminescence (PL) quantum yield for all benzimidazoles were measured in dichloromethane using coumarin 47 in ethanol as the standard. Single crystal XRD was recorded in Agilent Xcalibur Ruby Gemini diffractometer. Enhanced Mo X-ray source was

used as radiation source. Graphite monochromator with 10.5081 pixels mm⁻¹ was used as detector resolution.

2.2. General procedure for the catalytic synthesis of benzimidazole derivatives

A mixture of N-phenyl-*o*-phenylenediamine (1 mmol), corresponding aldehyde (1 mmol), ammonium acetate (2.5 mmol) and cobalt(II) hydroxide (10 or 15 mol %) was refluxed at 80° C in ethanol for different time intervals. The reaction was monitored by thin layer chromatography (TLC) and purified by column chromatography using petroleum ether as the eluent.

2.2.1. 1,2-Diphenyl-1H-benzo[d]imidazole (1)

Mp = 107°C, C₁₉H₁₄N₂: ¹H NMR (400 MHz, CDCl₃): δ 7.24-7.33 (q, 7H), 7.45-7.47 (d, 3H), 7.53-7.57 (d, 2H), 7.88-7.90 (d, 1H). ¹³C NMR (100 MHz, CDCl₃): δ 110.52, 119.89, 123.04, 123.39, 127.44, 128.35, 128.59, 129.26, 129.50, 129.90, 129.98, 137.00, 137.24, 143.03, 152.43. MS: m/e 271.26, calcd m/e 271.12 [M+1].

2.2.2. 2-(4-Fluorophenyl)-1-phenyl-1H-benzo[d]imidazole (2)

Mp = 96°C, C₁₉H₁₃FN₂: ¹H NMR (400 MHz, CDCl₃): δ 6.98-7.02 (t, 2H), 7.26-7.36 (m, 4H), 7.50-7.55 (m, 6H), 7.87-7.88 (d, 1H). ¹³C NMR (100 MHz, CDCl₃): δ 110.50, 115.44, 115.64, 119.83, 123.13, 123.47, 126.14, 126.18, 127.43, 128.75, 130.01, 131.41, 131.49, 136.84, 137.19, 142.90, 151.47, 162.16, 164.65. MS: m/e 289.17, calcd m/e 289.11 [M+1].

2.2.3. 2-(4-methylphenyl)-1-phenyl-1H-benzo[d]imidazole (3)

Mp = 111°C, C₂₀H₁₆N₂: ¹H NMR (400 MHz, CDCl₃): δ 2.33 (s, 3H), 7.09-7.11 (d, 2H), 7.24-7.26 (m, 2H), 7.30-7.32 (m, 3H), 7.44-7.50 (m, 5H), 7.87-7.89 (s, 1H). ¹³C NMR (100 MHz, CDCl₃): δ 21.42, 110.41, 119.73, 122.93, 123.18, 127.05, 127.48, 128.53, 129.07, 129.37, 129.88, 137.14, 137.24, 139.62, 143.02, 152.60. MS: m/e 285.30, calcd m/e 285.13 [M+1].

2.2.4. 2-(4-methoxyphenyl)-1-phenyl-1H-benzo[d]imidazole (4)

Mp = 118°C, C₂₀H₁₆N₂O: ¹H NMR (400 MHz, CDCl₃): δ 3.80 (s, 3H), 6.81-6.82 (d, 2H), 7.23-7.26 (m, 2H), 7.31-7.33 (m, 3H), 7.47-7.52 (m, 5H), 7.85-7.87 (s, 1H). ¹³C NMR (100 MHz, CDCl₃): δ 55.29, 110.32, 113.77, 119.55, 122.32, 122.89, 123.02, 127.50, 128.53, 129.90, 130.92, 137.21, 143.00, 152.41, 160.51. MS: m/e 301.21, calcd m/e 301.13 [M+1].

2.2.5. 2-(4-(Trifluoromethyl)phenyl)-1-phenyl-1H-benzo[d]imidazole (5)

Mp = 108°C, C₂₀H₁₃F₃N₂O: ¹H NMR (400 MHz, CDCl₃): δ 7.26-7.29 (m, 1H), 7.30-7.35 (m, 3H), 7.37-7.39 (m, 1H), 7.51-7.58 (m, 5H), 7.69-7.71 (d, 2H), 7.90-7.92 (d, 1H). ¹³C NMR (100 MHz, CDCl₃): δ 110.68, 120.15, 122.51, 123.40, 123.99, 125.25, 125.29, 125.33, 127.40, 129.01, 129.67, 130.16, 131.00, 131.32, 133.45, 136.61, 137.35, 142.90, 150.68. MS: m/e 339.38, calcd m/e 339.11 [M+1].

2.2.6. 2-(1-Phenyl-1H-benzo[d]imidazol-2-yl)phenol (6)

Mp = 114°C, C₁₉H₁₄N₂O: ¹H NMR (400 MHz, CDCl₃): δ 6.51-6.50 (t, 1H), 6.84-6.86 (d, 1H), 7.08-7.12 (q, 2H), 7.21-7.28 (m, 3H), 7.33-7.37 (t, 1H), 7.40-7.43 (m, 2H), 7.60-7.65 (m, 3H), 7.81-7.83 (d, 1H), 13.56 (s, 1H). ¹³C NMR (100 MHz, CDCl₃): δ 110.42, 112.37, 118.05, 118.06, 118.71, 123.48, 123.78, 127.33, 127.95, 129.58, 130.43, 131.45, 136.56, 137.21, 140.04, 150.82, 159.65. MS: m/e 287.26, calcd m/e 287.11 [M+1].

3. Results and discussion

3.1 Crystal structure of 2-(1-phenyl-1H-benzo[d]imidazol-2-yl)phenol (6)

2-(1-Phenyl-1H-benzo[d]imidazol-2-yl)phenol is a triclinic crystal and crystallizes in the space group $P\bar{1}$. The ORTEP diagram of **6** is presented in Figure 1. The benzimidazole unit is close to being planar [maximum deviation = 0.0253 (11) Å] and forms dihedral angles of 68.98 (6) and 20.38 (7)° with the adjacent phenyl and benzene rings; the dihedral angle between the latter two planes is 64.30 (7)°. In the crystal, molecules are linked by C—H...N

and C—H...O hydrogen bonds, and consolidated into a three-dimensional architecture by π - π stacking interactions, with a centroid – centroid distance of 3.8428 (12) Å [22]. Intramolecular hydrogen bonding shown by the ORTEP initiates us to study the ESIPT. Optimization of **6** have been performed by DFT at B3LYP/6-31G(d,p) level using Gaussian-03. All these XRD data are in good agreement with the theoretical values (Table S1). However, from the theoretical values it can be found that most of the optimized bond lengths, bond angles and dihedral angles are slightly higher than that of XRD values. These deviations can be attributed to the fact that the theoretical calculations are of isolated molecule in the gaseous phase and the XRD results are of the molecule in the solid state.

3.2. Effect of the catalytic activity of cobalt(II) hydroxide

Initially, we have carried out the condensation reaction of N-phenyl-*o*-phenylenediamine with substituted benzaldehyde in ethanol for 24 h with stirring, in the absence of catalyst and observed only trace amount of products. In order to improve the yield and shorten the reaction time, we have carried out the reaction using different amounts of the catalysts at different time intervals (Table 1). It was observed that the amount of catalyst plays a significant role in controlling the activity of the catalyst. Among the various amounts of catalyst used, 15 mol % was found to be the best in ethanol medium. A possible mechanism is that the reaction proceeds via the activation of aldehyde by Co(OH)₂ followed by imine formation. The resulted imine further reacts with another amine group of diamine leading to the formation of dihydroimidazole which subsequently undergoes aromatization under the oxidative conditions to give the benzimidazole as shown in Scheme 1. The present catalyst is novel and efficient. The salient features of this protocol are high product yields, shorter reaction time, low catalyst loading and easy work-up procedure, which make this procedure quite simple, more convenient and environmentally benign. Hopefully, our methodology

could be a valid contribution to the existing processes in the field of benzimidazoles synthesis.

3.3. Solvatochromism of benzimidazole derivatives (1-6)

Room temperature absorption and emission of benzimidazole derivatives (1-6) have been studied in different solvents and the spectra are displayed in Figures 2 and 3, respectively. Red shifts in the fluorescence bands of the benzimidazole derivatives were observed on increasing the solvent polarity. This is because the distortion of the geometry in the excited state which implies a decrease of the resonance energy; the fluorescence band is bathochromically shifted to a larger extent. Moreover, the loss of planarity in the excited state of the benzimidazole derivative could explain the lower fluorescence quantum yield in apolar solvents owing to an increase in the non-radiative processes. Blue shifts were observed with increase of solvent polarity in the absorption band of the benzimidazole derivatives. The shape of the absorption band is independent of the imidazole concentration suggesting the poor aggregation which is a required behavior for the performance of lasers [23].

A good linear correlation is obtained between the fluorescence maxima and the $E_T(30)$ values [24] (Figure 4a). Figure 4b is the constructed Lippert–Mataga plot [25] by using the relation

$$\nu_{SS} = [2(\mu_e - \mu_g) / hca^3] \Delta f + \nu_{SS}^o \quad (1)$$

where ν_{SS} is the Stokes shift, the superscript o indicates the absence of solvent, μ_g and μ_e are dipole moments in the ground state and excited state respectively and a is the Onsager cavity radius. The orientation polarizability Δf is defined as

$$\Delta f = [(\epsilon - 1) / (2\epsilon + 1)] - [(n^2 - 1) / (2n^2 + 1)] \quad (2)$$

where ϵ and n are solvent dielectric constant and refractive index, respectively. The geometrical optimization of benzimidazole derivatives was done by DFT method using Gaussian 03 software to calculate the μ_g [26]. Using the μ_g value, obtained from the DFT calculation [26], 3.36 D (1), 3.02 D (2), 3.38 D (3), 2.60 D (4), 3.40 D (5) and 3.06 D (6), and

the slope of Lippert–Mataga plot the value of μ_e is calculated. The calculated μ_e values are in the range of 12–14 D.

Effect of the variation of quantum yield (ϕ_f) with solvent polarity parameter $E_T(30)$ is shown in Figure 5a. It is clear from the plot that fluorescence quantum yield of benzimidazole derivatives decreases with increasing polarity of the solvents. The significant decreases of quantum yield observed upon increasing the protic nature of the medium suggest the differential contribution of charge transfer and hydrogen bonding interactions [27]. Radiative (k_r) and nonradiative (k_{nr}) rate constants are calculated from fluorescence quantum yield and lifetime values of benzimidazole derivatives in different solvents to understand the effect of solvation on the dynamics of the excited state. A typical set of k_r and k_{nr} values are given in Table 2. Figure 5b is the semi logarithmic plot of k_r/k_{nr} versus solvent polarity parameter $E_T(30)$. Upon increasing the polarity the logarithm ratio of radiative to nonradiative rate decreases. It indicates that the radiative and nonradiative rates are more sensitive toward protic solvents. It may be that the hydrogen bonding interaction in polar protic environments enhances the stabilization of the S1 state of benzimidazole derivatives; as a result, the nonradiative relaxation rate increases [27].

The free energy change of solvation and reorganization energies of **1-6** in various solvents have been estimated (Table 3). According to Marcus [28],

$E(A) = \Delta G_{solv} + \lambda_1$ and $E(F) = \Delta G_{solv} - \lambda_0$, where $E(A)$ and $E(F)$ are absorption and fluorescence band maxima in cm^{-1} , respectively, ΔG_{solv} is the difference in free energy of the ground and excited states in a given solvent and λ represents the reorganization energy. The free energy change of solvation and reorganization energies of **1-6** in various solvents have been estimated (Table 3). The definite values of reorganisation energy confirmed the interaction between low frequency motions such as reorientation of solvent cell with low and medium frequency nuclear motion of the solute. Under the condition that $\lambda_0 \approx \lambda_1 \approx \lambda$, we get,

$E(A) + E(F) = 2\Delta G_{\text{solv}}$; $E(A) - E(F) = 2\lambda$. The ΔG_{solv} of **1-6** is maximum for hexane since it is purely non-polar and also α and β values of hexane are zero. The ΔG_{solv} is minimum in water. The difference between these values (water and hexane) should give the free energy change required for hydrogen bond formation. The plot of $\Delta(\Delta G_{\text{solv}}) = (\Delta G_{\text{hex}} - \Delta G_{\text{water}})$ versus $E_T(30)$ is depicted in Figure 6a. The difference in free energy of solvation in hexane and different hydrogen bonding solvents, i.e., ΔG_{solv} of **1-6** follow the order of the hydrogen bond energy [29]. In the aprotic solvents the values are small and interaction of imidazole derivatives with those solvents is purely out of dipolar interactions in the excited state. The reorganization energy values of **1-6** have also been determined in different solvents.

The solvatochromic effects on the benzimidazole derivatives (**1-6**) were analysed by employing the multilinear expression proposed by Catalan. It involves a generalized treatment of the solvent effect based on the acidity (SA), basicity (SB), polarizability (SP), and dipolarity (SdP) given in the following equation [30, 31],

$$y = y_o + a SA + b SB + c SP + d SdP \quad (3)$$

where y_o represents the physiochemical property of interest in the gas phase; a , b , c and d are the estimated coefficients that describe the dependence of the physiochemical property. Table 4 presents the coefficients of multi-parameter correlation. The absorption and fluorescence bands of the benzimidazoles show that the solvatochromic shifts are associated with the solvent polarity. The emission of imidazole derivative with *p*-tolyl, *p*-methoxy and *p*-trifluoromethyl substituents is less affected by the H-donor capacity of the solvent. The absorbance of all the imidazole derivatives studied is insensitive to the electron releasing ability or basicity of the solvent (C_β or C_{SB}). However, *p*-fluoro- and *o*-hydroxy-substituted imidazoles along with the parent molecule are highly susceptible to the H-donor capacity of the solvent. The susceptibility of the hydroxy compound is double that of *p*-fluoro benzimidazole and the parent benzimidazole derivatives. The large solvatochromic effect

shown by the hydroxyl molecule is due to intermolecular hydrogen bonding. The less significant solvent effect experienced by *p*-methyl, *p*-methoxy and *p*-trifluoromethyl-substituted molecules cannot be due to electronic effect but may be because of steric effect.

Figure 6b presents the possible resonance stabilization of the studied molecules. In the case of *p*-fluoro substituted molecule and the parent molecule the charge on the phenyl carbon attached to the substituent could be stabilized by acidic solvents but the same is sterically hindered by *p*-methyl, *p*-methoxy and *p*-trifluoromethyl substituents. This resonance structure is predominant in the S_1 state and the stabilization of the S_1 state with the H-donor capacity of the solvent is more important than that of the S_0 state. Consequently, the energy gap between S_1 and S_0 states is decreased. With increase of the H-donor capacity of the solvent, fluorescence are shifted to longer wavelengths which explains the solvatochromic shifts.

An interesting result is provided by the blue shift of the CT absorption bands with increasing solvent polarity (Figure 7a) [32, 33]. With the assumption that point dipole is at the center of the spherical cavity and the mean solute polarizability (α) to be insignificant, it follows,

$$hc\nu_{\text{abs}} \approx hc\nu_{\text{abs}}^{\text{vac}} - 2 \mu_g (\mu_e - \mu_g) / a_0^3 [(\epsilon - 1/2 \epsilon + 1) - 1/2 (n^2 - 1/2n^2 + 1)] \quad (4)$$

where μ_g and μ_e are the dipole moments of the solute in the ground and excited states, correspondingly, ν_{abs} and $\nu_{\text{abs}}^{\text{vac}}$ are the spectral positions of a solvent-equilibrated absorption maxima and the value extrapolated to the gas-phase, respectively, a_0 is the effective radius of the Onsager cavity, [34] and ϵ and n are the static dielectric constant and the refractive index of the solvent, respectively. In the case of CT absorption bands, eqn 4 is used to determine the values of $\mu_g (\mu_e - \mu_g) / a_0^3$ and $\nu_{\text{abs}}^{\text{vac}}$. The linear correlation reveal that the blue shift of the CT absorption band is probably due to the fact that the dipolar molecule cannot be approximated by the point dipole situated in the center of the cavity. The ground state dipole moment is mostly determined by polar fragment of benzimidazole derivatives lying far from the center of the molecule (Figure 7b). It leads to an increase of the effective Onsager

reaction field [35] and to a corresponding increase in the ground state solvation energies and blue shift observed in the absorption spectra. In the excited state, the negative and positive ends of the electric dipole are localised nearly in the centres of the donor and acceptor fragments of the benzimidazole derivatives, respectively (Figure 7b). In fluorescence spectra, the observed red shift and the increase of the Stokes shift with increasing solvent polarity clearly indicate that the absolute values of μ_e are much higher than those of μ_g [36-38]. Under the same assumption as used for expression 4, it follows that

$$hc\nu_{\text{flu}} \approx hc\nu_{\text{flu}}^{\text{vac}} - 2\mu_e(\mu_e - \mu_g) / a_0^3 [(\epsilon - 1/2\epsilon + 1) - 1/2(n^2 - 1/2n^2 + 1)] \quad (5)$$

where, ν_{flu} and $\nu_{\text{flu}}^{\text{vac}}$ are the spectral positions of the solvent equilibrated fluorescence maxima and the value extrapolated to the gas-phase, respectively. The compounds studied show a satisfying linear correlation between the energy $hc\nu_{\text{flu}}$ and the solvent polarity function in a polar environment and also in all the solvents studied [39] (Figure 7c) the values of $\mu_e(\mu_e - \mu_g) / a_0^3$ are displayed in Table 5. The values, extracted from the data measured in polar media, are somewhat larger than those resulting from the analysis of the data obtained for the whole range of the solvents. This finding can be explained only by the dependence of the electronic structure of the fluorescent states on solvation. Due to a relatively small energy gap between the lowest internal charge transfer (ICT) states and the states excited locally in the nonpolar solvents, which leads to increase of the contribution of the (π, π^*) character to the wave function of the CT states. It leads to a lowering of energy with respect to a pure CT state because of a stabilizing character of such interactions and red shift obtained in the fluorescence spectra.

Under the assumption that the CT fluorescence corresponds to the state reached directly upon excitation, the quantity $(\mu_e - \mu_g)^2 / a_0^3$ can be evaluated from the solvation effects on the Stokes shift,

$$hc(\lambda_{\text{abs}} - \lambda_{\text{flu}}) = hc\left(\frac{hc\nu_{\text{abs}}^{VAC}}{a_0^3} - \frac{hc\nu_{\text{flu}}^{VAC}}{a_0^3}\right) + 2(\mu_e - \mu_g)^2 / a_0^3 \left[(\epsilon - 1/2\epsilon + 1) - 1/2(n^2 - 1/2n^2 + 1) \right] \quad (6)$$

The compounds studied show a satisfying linear correlation between the energy $hc\lambda_{\text{abs}} - hc\lambda_{\text{flu}}$ and the solvent polarity function in a polar environment and also in all the solvents studied, the values of $(\mu_e - \mu_g) / a_0^3$ are 1.407 eV (1), 1.509 eV (2), 1.115 eV (3), 1.358 eV (4), 1.362 eV (5) and 1.023 eV (6). The equations 4-6 relate the measured quantities to the excited state dipole moments μ_e . Under the assumption that $\mu_e \gg \mu_g$ and with the effective spherical radius of the molecules a_0 , 5.21 Å (1), 5.27 Å (2), 5.30 Å (3), 5.39 Å (4), 5.52 Å (5) and 5.29 Å (6), as estimated from the molecular dimensions of the compounds calculated by molecular mechanics, equations 5 and 6 yield very similar values of μ_e being in the range of 12.4 D (1), 13.08 D (2), 13.20 D (3), 12.83 D (4), 12.32 D (5) and 10.84 D (6) for the studied molecules.

3.4. ESIPT process

The emission spectra of 2-(1-Phenyl-1H-benzo[d]imidazol-2-yl)phenol (6) in dioxane exhibit a dual emission. Excitation of isomer I lead to the formation of keto-isomer II shown in Figure 8. The dual emission is due to ESIPT displayed in Figure 9. However, in hydroxylic solvent a short wavelength emission band appears for 6 which is absent in the emission spectra of other molecules (Figure 3). This result is similar to those reported in literature [40]. Absence of dual emission by 6 in hydroxyl solvents is explained by the presence of intermolecular hydrogen bonding with solvent molecule leading to the stabilization of solvated isomer III in which ESIPT is impossible.

Existence of ESIPT mechanism in hydroxybenzimidazole derivative, 2-(1-Phenyl-1H-benzo[d]imidazol-2-yl) phenol (6) is supported by DFT calculations. The electron density of keto and enol isomers of 6 in the ground and excited states calculated by B3LYP/6-31G(d,p) method is presented in Table 6. Excitation of enol isomer leads to increase of the electron density at azomethine nitrogen atom (3) and decrease of the same at oxygen atom (26)

resulting ESIPT. As a consequence of ESIPT, excited keto isomer is formed. The excited keto isomer returns to the ground state keto form (III) with the emission of luminescence. This is supported by DFT analysis which provides a large positive charge at N(3) nitrogen atom and negative charge at oxygen atom. As a result, a reverse process occurs in the ground state of the molecule producing enol form. The electron density at azomethine nitrogen (3) of structure II is increased on excitation. The electron density of II and II* are -0.395 e.u and -0.455 e.u respectively. i.e., the basicity is enhanced on excitation. Similarly the acidity is decreased on excitation. The electron density at oxygen (26) of structure II decreases from -0.570 to -0.528 i.e., the acidity is increased.

3.5. Driving force for ESIPT process

The existence of intramolecular hydrogen bonding in 2-(1-Phenyl-1H-benzo[d]imidazol-2-yl)phenol (**6**) is confirmed by single crystal XRD (Figure 1) and also by the presence of singlet at 13.56 ppm in the ^1H NMR spectrum shown in (Figure 10), which is a typical signal for hydrogen bonded hydrogen atom. The fluorescence spectra of **6** and benzimidazole derivative **1** (not having hydroxyl group) in dioxane under identical condition reveal the contribution of the intramolecular hydrogen bonding in **6**. A dual fluorescence is exhibited by **6** whereas other compounds exhibit only single emission. The emission of **6** at shorter wavelength is assigned to rotamer I and that at the longer wavelength is assigned to rotamer II. The absence of additional peak in **1-5** confirms absence of intramolecular hydrogen bond. It is further evident that intramolecular hydrogen bonding is the driving force for ESIPT and dual fluorescence behaviour of **6**.

3.6. HOMO-LUMO electron density vs ESIPT

The electron density of HOMO and LUMO of 2-(1-Phenyl-1H-benzo[d]imidazol-2-yl)phenol (**6**) shown in Figure 11 can throw some light on the excited state proton transfer processes. The HOMO of enol form predicts that intramolecular hydrogen bonded (IMHB) ring system

possess bonding character over the O(26) H(26) and C(2) C(21) atoms. Both oxygen O(26) and azomethine nitrogen N(3) have bonding character and the electron density on oxygen (O26) is large. The electron density of HOMO of keto tautomer around IMHB ring shows antibonding character over the C(26) O(26) and N(3) H(26). Again, comparison of the HOMOs of enol and keto forms shows that the electron density at the oxygen of keto form is large. The HOMO electron density of both the enol and keto forms indicates less electron density over the phenyl ring. By considering the LUMO of enol and keto forms, LUMO of the enol tautomer possesses high electron density on azomethine N(3). After tautomerization, the LUMO of keto-tautomer still shows larger electron density on azomethine nitrogen and comparatively smaller density on oxygen. Thus it favours the transfer of a proton from oxygen to azomethine nitrogen in the excited state. Again our calculation of electron density over the proton transfer co-ordinate in the excited states (*i.e.*, LUMO electron densities) shows that there is a shift of π -electron distribution from O(26) to azomethine N(3). Analysis of the electron density of HOMO for enol tautomer predicts that azomethine nitrogen N(3) has slightly higher bonding character than oxygen. On the other hand, HOMO electron density of keto tautomer shows greater bonding character of oxygen than azomethine nitrogen and hence transfer of proton from oxygen O(26) to azomethine nitrogen N(3) in the ground state is quite impossible.

3.7. Fluorescence lifetime and quantum yield

The time correlated single photon counting (TCSPC) results fit to single exponentials decay (Figure 12), DAS6 software was used for the fit and the χ^2 values are less than 1.2. The fluorescence lifetime measurements of all benzimidazole derivatives were made with laser excitation set at 270 nm and the fluorescence signal was measured at the emission wavelength of individual compound. The deduced parameters are listed in Table 2. The absolute PL quantum yields were measured by comparing fluorescence intensities (integrated

areas) of a standard sample (Coumarin 46) and the unknown sample using the formula

$$\Phi_{\text{unk}} = \Phi_{\text{std}} \left(\frac{I_{\text{unk}}}{I_{\text{std}}} \right) \left(\frac{A_{\text{std}}}{A_{\text{unk}}} \right) \left(\frac{\eta_{\text{unk}}}{\eta_{\text{std}}} \right)^2$$

where, Φ_{unk} is the fluorescence quantum yield of the sample, Φ_{std} is the fluorescence quantum yield of the standard; I_{unk} and I_{std} are the integrated emission intensities of the sample and the standard, respectively. A_{unk} , and A_{std} are the absorbances of the sample and the standard at the excitation wavelength, respectively. η_{unk} and η_{std} are the indexes of refraction of the sample and standard solutions. The radiative and non-radiative decay of the excited state of **1-6** have been obtained using the quantum yields and lifetimes and are listed in Table 2. The formula employed to calculate the radiative (k_r) and non-radiative (k_{nr}) rate constants is $k_r = \Phi_p/\tau$; $k_{nr} = (1/\tau) - (\Phi_p/\tau)$; $\tau = (k_r + k_{nr})^{-1}$, where k_r and k_{nr} are the radiative and non-radiative deactivation, τ_f is the lifetime of the S_1 excited state. Table 2 shows that all the molecules synthesized have moderate quantum yields. Perusal of the radiative and non-radiative rate constants shows that in most of the cases the radiative emission is predominant over non-radiative transitions. Furthermore, Table 2 shows that the non-radiative rate constants of the methyl and methoxy substituted molecules are larger than those of the others. This could be the electron releasing nature of the methyl and methoxy substituents.

4. Conclusion

In this article we report an elegant synthesis of some fluorescent benzimidazole derivatives under mild reaction conditions with inexpensive cobalt(II) hydroxide as catalyst. In addition, the overall yields of the compounds are not less than 75%, is a promising synthesis for scaling up. Observed blue shift of absorption CT band and red shift of emission band have been discussed. The difference in free energy of solvation in polar protic and aprotic solvent corresponds to the hydrogen bond energy. The compounds studied show a satisfying linear correlation between the energy $hc\lambda_{\text{abs}}$, $hc\lambda_{\text{flu}}$, $hc\lambda_{\text{abs}} - hc\lambda_{\text{flu}}$ and the solvent polarity function in a polar environment. All the studied compounds are having moderate quantum

efficiency. Excited state depopulation kinetic studies have also been carried out. Hydroxy-substituted benzimidazole shows a single prominent emission in polar solvents and dual emission in non-polar solvents due to ESIPT. HOMO- LUMO analysis and crystal structure support the ESIPT.

Acknowledgments

One of the authors Prof. J. Jayabharathi is thankful to DST [No. SR/S1/IC-73/2010] and DRDO (NRB-213/MAT/10-11) for providing funds to this research study. Mr. K. Jayamoorthy is thankful to DST [No. SR/S1/IC-73/2010] for providing fellowship.

References

- [1] E.M. Across, K.M. White, R.S. Moshrefzadeh, C.V. Francis, Azobeneimidazole compounds and polymers for nonlinear optics, *Macromolecules* 28 (1995) 2526-2532.
- [2] G.A. Jeffrey, *An Introduction to Hydrogen Bonding*, Oxford University Press, Oxford, England, 1997.
- [3] L. Pauling, The nature of the chemical bond. Application of results obtained from the quantum mechanics and from a theory of paramagnetic susceptibility to the structure of molecules, *J. Am. Chem. Soc.* 53 (1931) 1367.
- [4] G.R. Desiraju, T. Steiner, *The Weak Hydrogen Bond in Structural Chemistry and Biology*, Oxford University Press, New York, 1999.
- [5] J. Jayabharathi, V. Thanikachalam, K. Jayamoorthy, Physicochemical studies of chemosensor imidazole derivatives: DFT based ESIPT process, *Spectrochim. Acta Part A*: 89 (2012) 168-176.
- [6] J. Jayabharathi, V. Thanikachalam, M. Vennila, K. Jayamoorthy, Potential fluorescent chemosensor based on L-tryptophan derivative: DFT based ESIPT process, *Spectrochim. Acta A*. 95 (2012) 446-451.
- [7] P.T. Chou, M.L. Martinez, J.H. Clements, Reversal of Excitation Behavior of Proton-transfer vs. Charge- Transfer by Dielectric Perturbation of Electronic State Manifolds, *J. Phys. Chem.* 97 (1993) 2618–2622.
- [8] L.F. Campo, F.S. Rodembusch, V. Stefani, New fluorescent monomers and polymers displaying an intramolecular proton-transfer mechanism in the electronically excited state (ESIPT). IV. Synthesis of acryloylamide and diallylamino benzazole dyes and its copolymerization with MMA, *J. Appl. Polym. Sci.* 99 (2006) 2109–2116.

- [9] Y. Wu, X. Peng, J. Fan, S. Gao, M. Tian, J. Zhao, S. Sun, Fluorescence Sensing of Anions Based on Inhibition of Excited-State Intramolecular Proton Transfer, *J. Org. Chem.* 72 (2007) 62–70.
- [10] S. Park, O.H. Kwon, Y.S. Lee, D.J. Jang, S.Y. Park, Imidazole-Based Excited-State Intramolecular Proton-Transfer (ESIPT) Materials: Observation of Thermally Activated Delayed Fluorescence (TDF), *J. Phys. Chem. A* 111 (2007) 9649–9653.
- [11] O.K. Abou-Zied, R. Jimenez, F.E. Romesberg, Tautomerization dynamics of a model base-pair in DNA, *J. Am. Chem. Soc.* 2001, 123, 4613- 4614.
- [12] W.S. Yu, C.C. Cheng, Y.M. Cheng, P.C. Wu, Y.H. Song, Y. Chi, P.T. Chou, Excited state intra molecular proton transfer in five membered hydrogen bonding system: 2-pyridyl pyrazoles, *J. Am. Chem. Soc.* 2003, 125, 10800-10801.
- [13] C.L. Chen, C.W. Lin, C.C. Hsieh, C.H. Lai, G.H. Lee, C.C. Wang, P.T. Chou, Dual Excited-State Intramolecular Proton Transfer Reaction in 3-Hydroxy-2-(pyridin-2-yl)-4H-chromen-4-one, *J. Phys. Chem. A* 2009, 113, 205-214.
- [14] K.Y. Chen, C.C. Hsieh, Y.M. Cheng, C.H. Lai, P.T. Chou, Extensive spectral tuning of the proton transfer emission from 550 to 675 nm via a rational derivatization of 10-hydroxybenzo[h]quinoline, *Chem. Commun.* 2006, 42, 4395-4397.
- [15] K.Y. Chen, Y.M. Cheng, C.H. Lai, C.C. Hsu, M.L. Ho, G.H. Lee, P.T. Chou, Ortho green protein synthetic chromophore; Excited-state intramolecular proton transfer via a six membered ring hydrogen bonding system, *J. Am. Chem. Soc.* 2007, 129, 4534-4535.
- [16] E.M. Itskovitch, J. Ulstrup, M.A. Vorotyntsev, in: R.R. Dogonadze, E. Kalman, A.A. Kornyshev, J. Ulstrup(Eds.), *The chemical physics of solvation part B*, Elsevier, Amsterdam, 1986.

- [17] A. Siemiarzuk, Z.R. Grabowski, A. Kro'wczyn'ski, M. Asher, M. Ottolenghi, Two emitting states of excited p-(9-anthryl)-N,N-dimethylaniline derivatives in polar solvents, *Chem. Phys. Lett.*, 1977, 51, 315-320.
- [18] A. Siemiarzuk, W.R. Ware, Complex excited state relaxation in p(9-Anthryl)-N,N-dimethylaniline derivative evidenced by fluorescence lifetime distributions, *J. Phys. Chem.* 1987, 91, 3677-3682.
- [19] K. Tominaga, G.C. Walker, W. Jarzeü ba, P.F. Barbara, Ultrafast charge separation in ADMA: experiment and theoretical issues, *J. Phys. Chem.* 1991, 95, 10475-10485.
- [20] K. Tominaga, G.C. Walker, T.J. Kang, P.F. Barbara, T. Fonseca, Reaction rates in the phenomenological adiabatic excited-state electron-transfer theory, *J. Phys. Chem.* 1991, 95, 10485-10492.
- [21] T. Okada, N. Mataga, W. Baumann, A. Siemiarzuk, Picosecond laser spectroscopy of 4-(9-Anthryl-) N,N-dimethylaniline and related compounds, *J. Phys. Chem.* 1987, 91, 4490-4495.
- [22] A. Thiruvalluvar, S. Rosepriya, K. Jayamoorthy, J. Jayabharathi, S. O. Yildirim, and R. J Butcher, 2-(1-Phenyl-1H-benzimidazol-2-yl)phenol, *Acta Cryst. E*69, 2013, o62.
- [23] I. Lopez Arbeloa, Fluorescence quantum yield evaluation: corrections for re-absorption and re-emission, *J. Photochem.* 14 (1980) 97-105.
- [24] C. Reichardt, Empirical parameters of solvent polarity as linear free energy relationships, *Angew. Chem., Int. Ed. Engl.*, 1979, 18, 98-110.
- [25] E. Lippert, Spektroskopische bistimmung des dipolmomentes aromatischer verbindugenim ersten angeregten singulettzustand, *Z. Electrochem.*, 1957, 61, 962-975.
- [26] M. J. Frisch, G. W. Trucks, H. B. Schlegel, G. E. Scuseria, M. A. Robb, J. R. Cheeseman, J. A. Montgomery, Jr., T. Vreven, K. N. Kudin, J. C. Burant, J. M. Millam, S. S. Iyengar, J. Tomasi, V. Barone, B. Mennucci, M. Cossi, G. Scalmani, N. Rega, G.

- A. Petersson, H. Nakatsuji, M. Hada, M. Ehara, K. Toyota, R. Fukuda, J. Hasegawa, M. Ishida, T. Nakajima, Y. Honda, O. Kitao, H. Nakai, M. Klene, X. Li, J. E. Knox, H. P. Hratchian, J. B. Cross, V. Bakken, C. Adamo, J. Jaramillo, R. Gomperts, R. E. Stratmann, O. Yazyev, A. J. Austin, R. Cammi, C. Pomelli, J. W. Ochterski, P. Y. Ayala, K. Morokuma, G. A. Voth, P. Salvador, J. J. Dannenberg, V. G. Zakrzewski, S. Dapprich, A. D. Daniels, M. C. Strain, O. Farkas, D. K. Malick, A. D. Rabuck, K. Raghavachari, J. B. Foresman, J. V. Ortiz, Q. Cui, A. G. Baboul, S. Clifford, J. Cioslowski, B. B. Stefanov, G. Liu, A. Liashenko, P. Piskorz, I. Komaromi, R. L. Martin, D. J. Fox, T. Keith, M. A. Al-Laham, C. Y. Peng, A. Nanayakkara, M. Challacombe, P. M. W. Gill, B. Johnson, W. Chen, M. W. Wong, C. Gonzalez and J. A. Pople, Gaussian 03 (Revision E.01), Gaussian, Inc., Wallingford, CT, 2004.
- [27] S. Dhar, D. K. Rana, S. S. Roy, S. Roy, S. Bhattacharya and S. C. Bhattacharya, Effect of solvent environment on the photophysics of a newly synthesized bioactive 7-oxy(5-selenocyanato-pentyl)-2H-1-benzopyran-2-one, *J. Lumin.*, 2012, 132, 957–964.
- [28] R.A. Marcus, Free Energy of Non equilibrium Polarization Systems. II. Homogeneous and Electrode Systems, *J. Chem. Phys.* 38 (1963) 1858.
- [29] G.W. Castellan, *Physical Chemistry*, third edition, Narosa Publishing House, Delhi, 1985.
- [30] M.J. Kamlet, R.W. Taft, The solvatochromic comparison method. 1. The scale of solvent hydrogen-bond acceptor (HBA) basicities, *J. Am. Chem. Soc.* 1976, 98, 377-383.
- [31] J. Catalan, V. Lopez, P. Perez, Use of the SPP scale for the analysis molecular system with dual emissions resulting from the solvent polarity, *J. Fluoresc.* 1996, 6, 15-22.
- [32] W. Rettig, M. Zander, On Twisted Intramolecular Charge Transfer (TICT) stated in N-aryl-carbazoles, *Chem. Phys. Lett.* 1982, 87, 229-234.
- [33] K. Chiba, J.I. Aihara, K. Araya, Y. Matsunaga, *Bull. Chem. Soc. Jpn.* 1980, 53, 1703.

- [34] L. Onsager, Electric moments of molecules in liquids, *J. Am. Chem. Soc.* 1936, 58, 1486-1493.
- [35] C.J.F. Boëtcher, O.C. Van Belle, P. Bordewijk, A. Rip, In *Theory of Electric Polarization*, Eds.; Elsevier: Amsterdam, 1973; Vol. I.
- [36] E.Z. Lippert, *Naturforsch.* 1955, A10, 541-546.
- [37] N. Mataga, Y. Kaifu, M. Koizumi, *The Solvent Effect on Fluorescence Spectrum. Change of Solute-Solvent Interaction During the Lifetime of Excited Solute Molecule*, *Bull. Chem. Soc. Jpn.* 1955, 28, 690-691.
- [38] W. Liptay, In *Excited States*; Lim, E. C., Ed.; Academic Press: New York, 1974; p 129.
- [39] E.G. McRae, *Theory of solvent effects on molecular electronic spectra. Frequency shifts*, *J. Phys. Chem.* 1957, 61, 562-572.
- [40] J. Jayabharathi, V. Thanikachalam, K. Jayamoorthy, N. Srinivasan, *Synthesis, spectral studies and solvatochromism of some novel benzimidazole derivatives – ESIPT process*, *Spectrochim. Acta Part A*: 105 (2013) 223-228.

Figure Captions

Figure 1. ORTEP diagram of 2-(1-phenyl-1H-benzo[d]imidazol-2-yl)phenol

Figure 2. Absorption spectra of **1-6** in different solvents

Figure 3. Emission spectra of **1-6** in different solvents

Figure 4. (a) Fluorescence maxima and the $E_T(30)$; (b) Lippert–Mataga plot

Figure 5. (a) Quantum yield with $E_T(30)$; (b) $\log(k_r/k_{nr})$ Vs $E_T(30)$

Figure 6. (a) Δ (ΔG_{solv}) Vs $E_T(30)$; (b) Resonance structure of the Chromophoric cores

Figure 7. (a) CT Absorption maxima Vs solvent polarity function; (b) Direction of ground and excited state dipole; (c) CT Fluorescence maxima Vs solvent polarity function

Figure 8. Various tautomeric and solvated forms of **6**

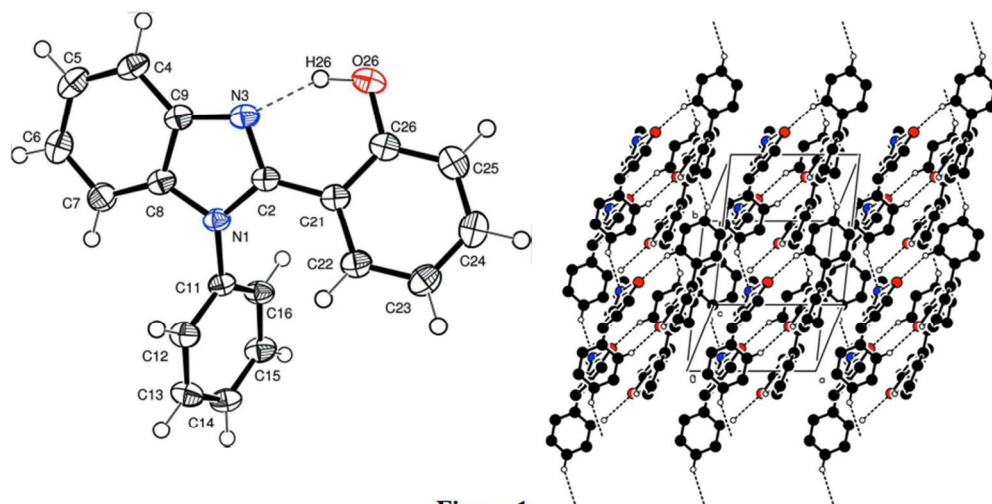
Figure 9. Suggested ESIP and interconversion mechanism

Figure 10. Proton NMR spectrum of 2-(1-phenyl-1H-benzo[d]imidazol-2-yl)phenol

Figure 11. HOMO-LUMO contour maps calculated by DFT/B3LYP/6-31G(d,p)

Figure 12. Time resolved single exponential decay curves

Scheme.1. Possible mechanism of catalytic synthesis of benzimidazoles

**Figure 1**

247x128mm (96 x 96 DPI)

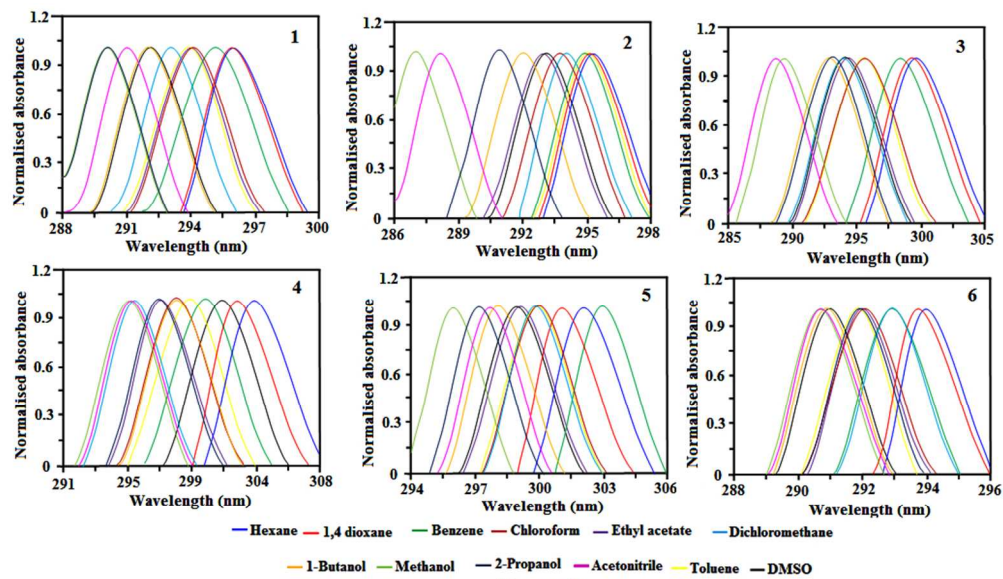


Figure 2

273x165mm (96 x 96 DPI)

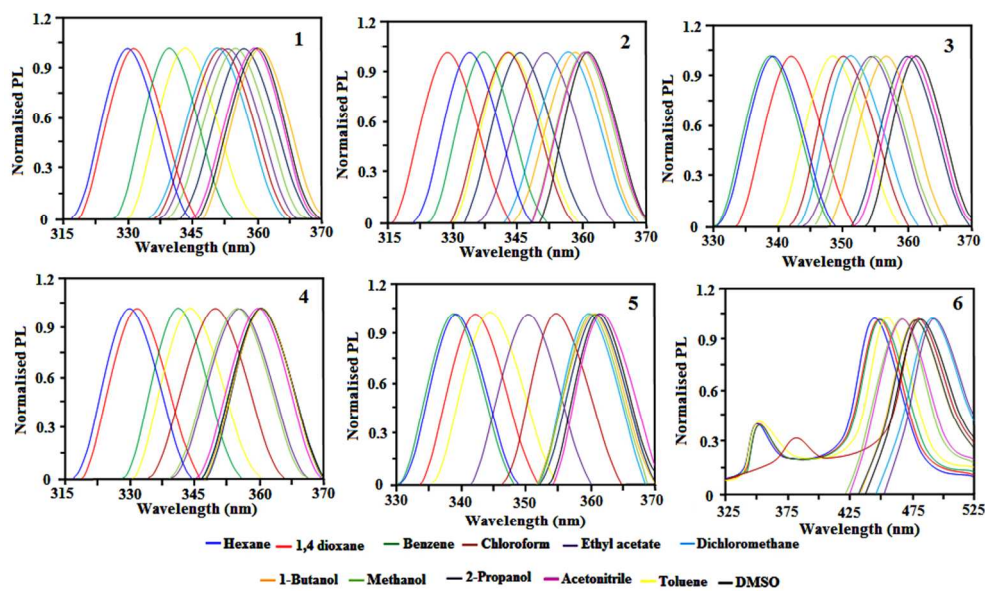


Figure 3

276x168mm (96 x 96 DPI)

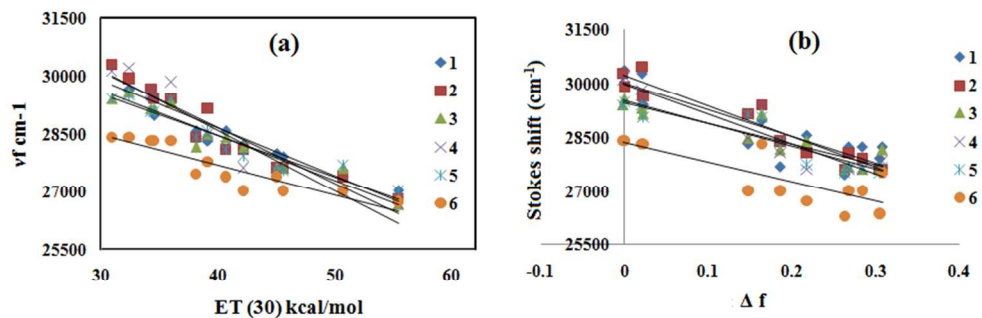


Figure 4

239x89mm (96 x 96 DPI)

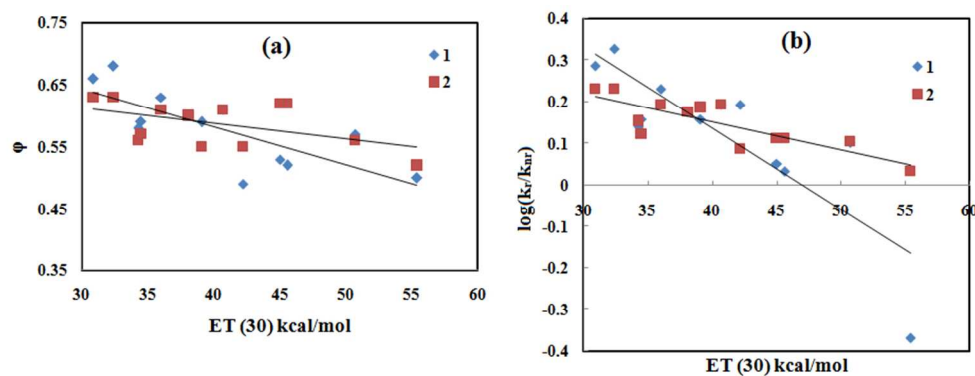
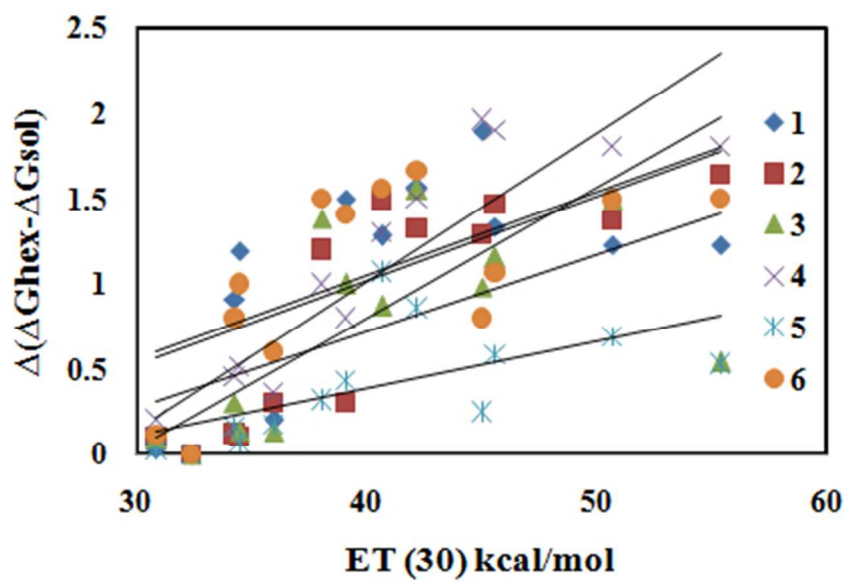
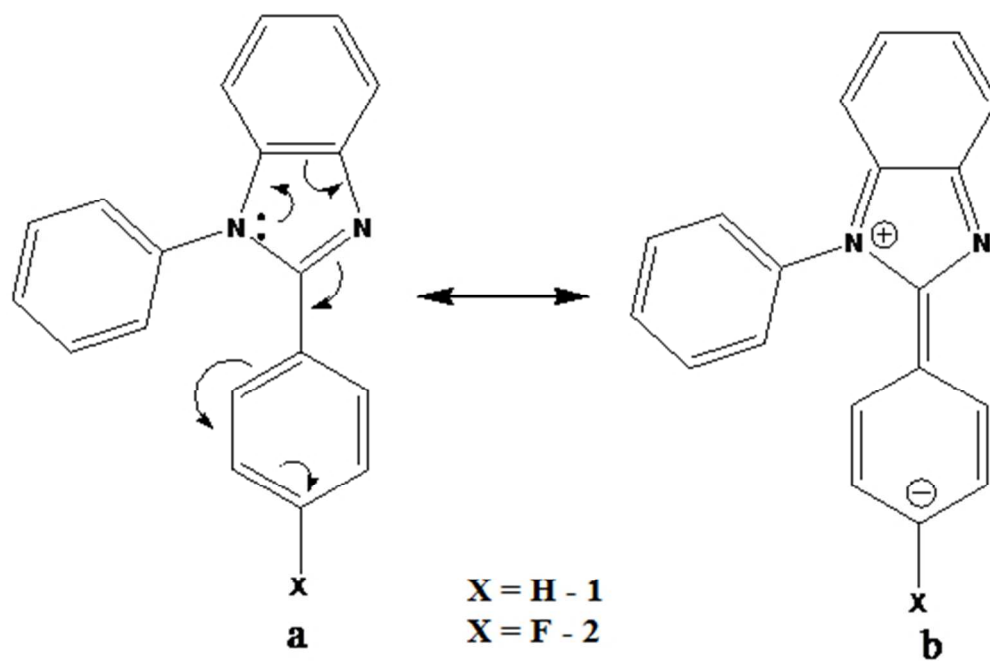


Figure 5

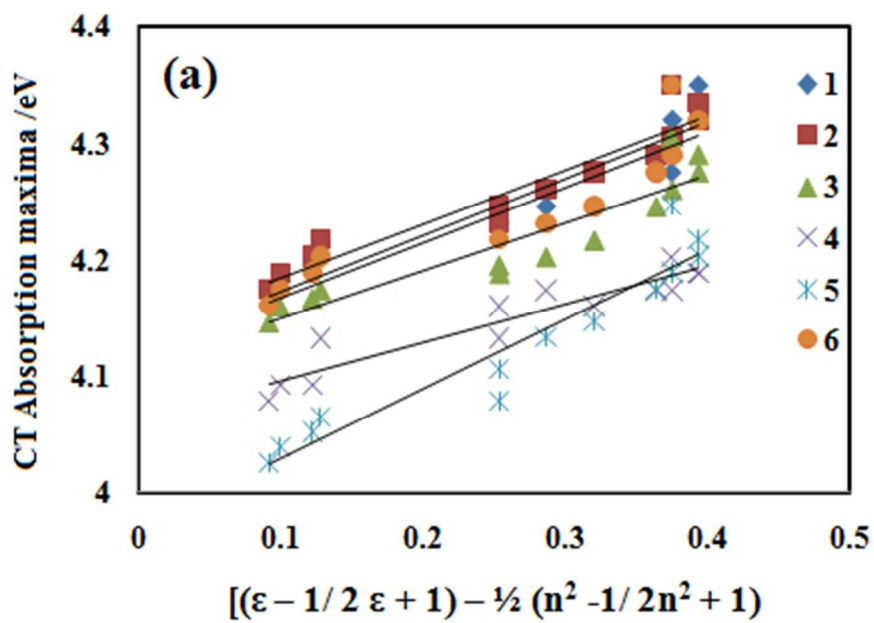
250x102mm (96 x 96 DPI)

**Figure 6a**

119x93mm (96 x 96 DPI)

**Figure 6b**

142x108mm (96 x 96 DPI)

**Figure 7a**

125x98mm (96 x 96 DPI)

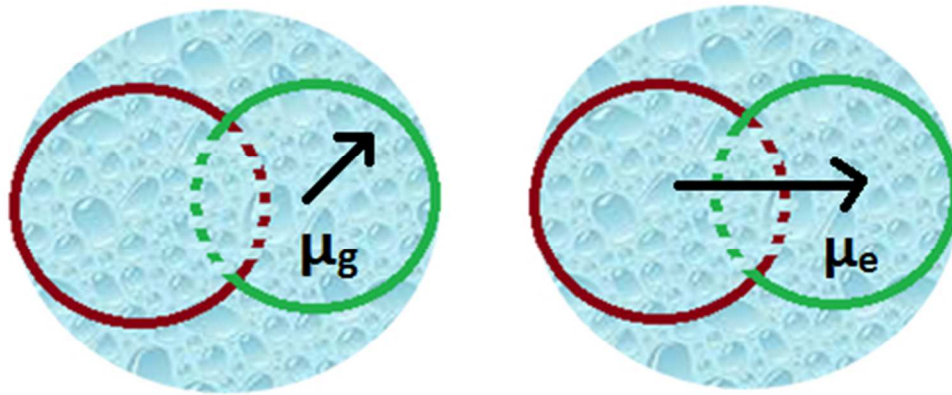
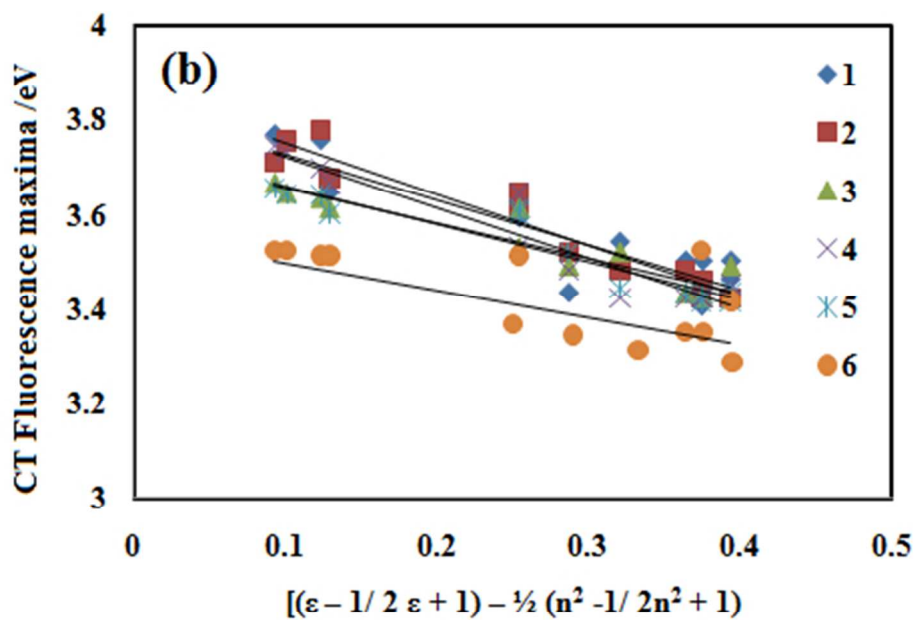
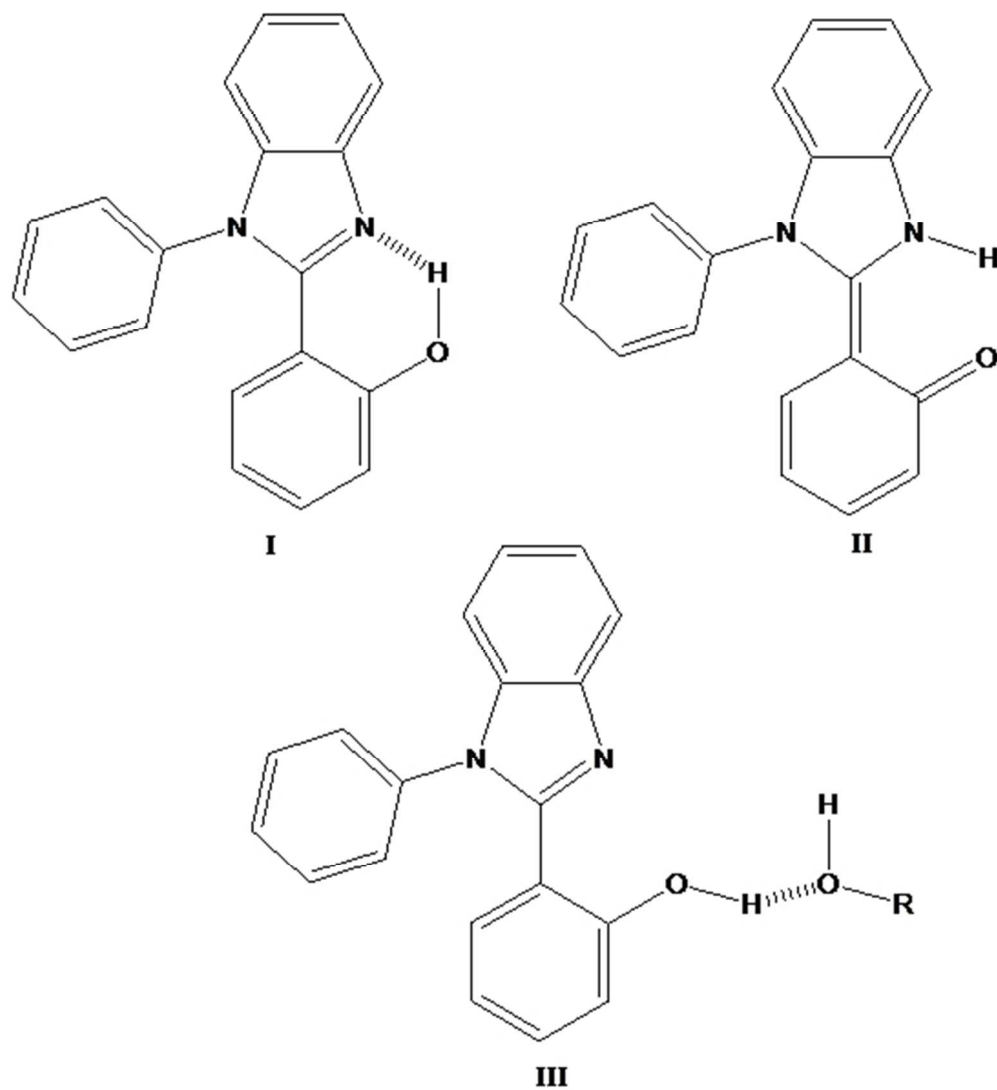


Figure 7b

135x75mm (96 x 96 DPI)

**Figure 7c**

131x97mm (96 x 96 DPI)

**Figure 8**

145x171mm (96 x 96 DPI)

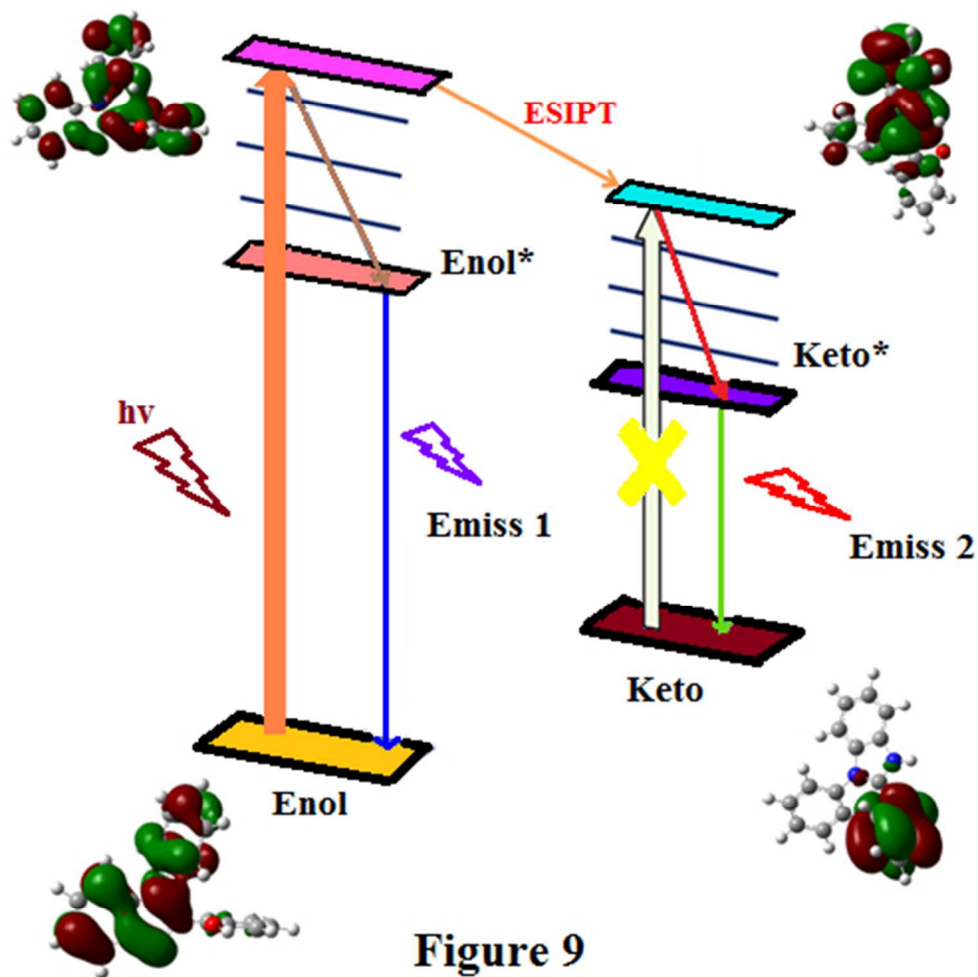


Figure 9

133x134mm (96 x 96 DPI)

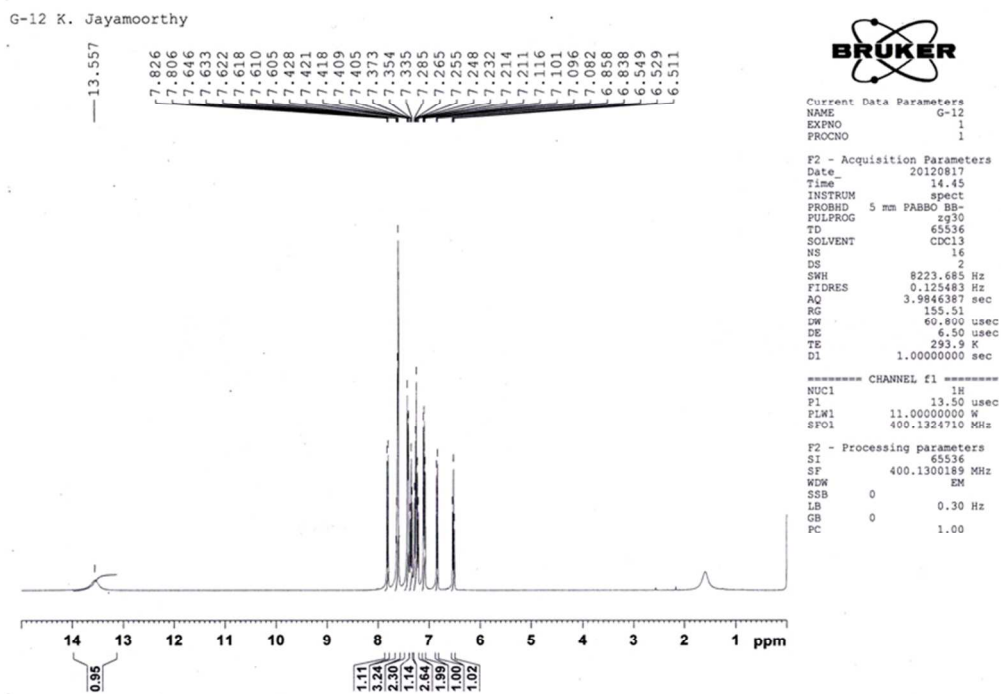
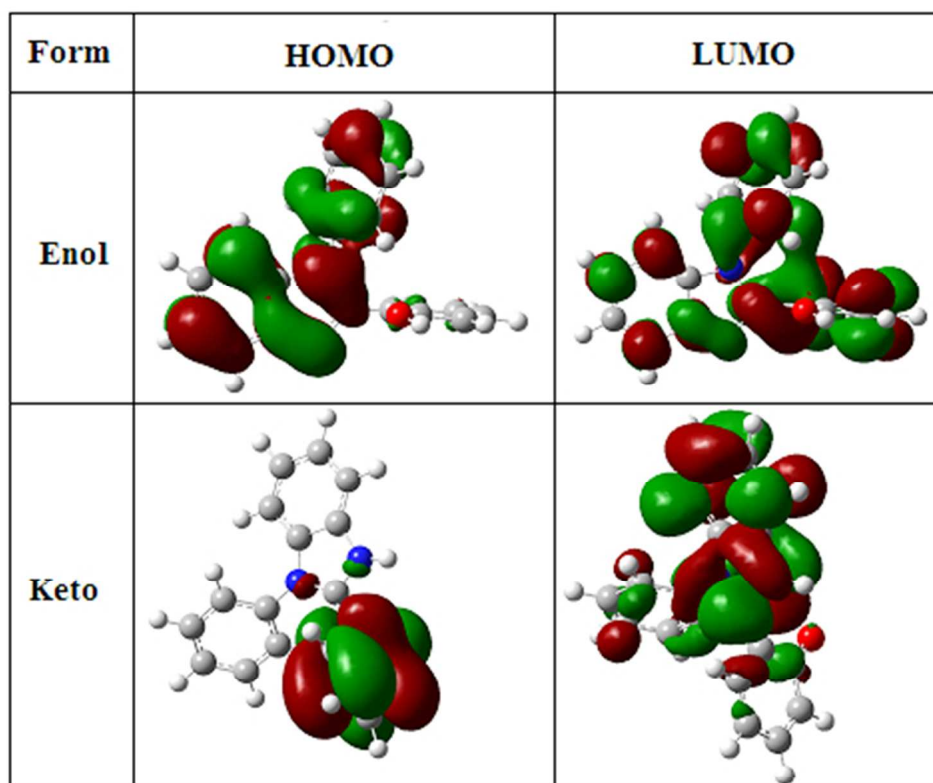
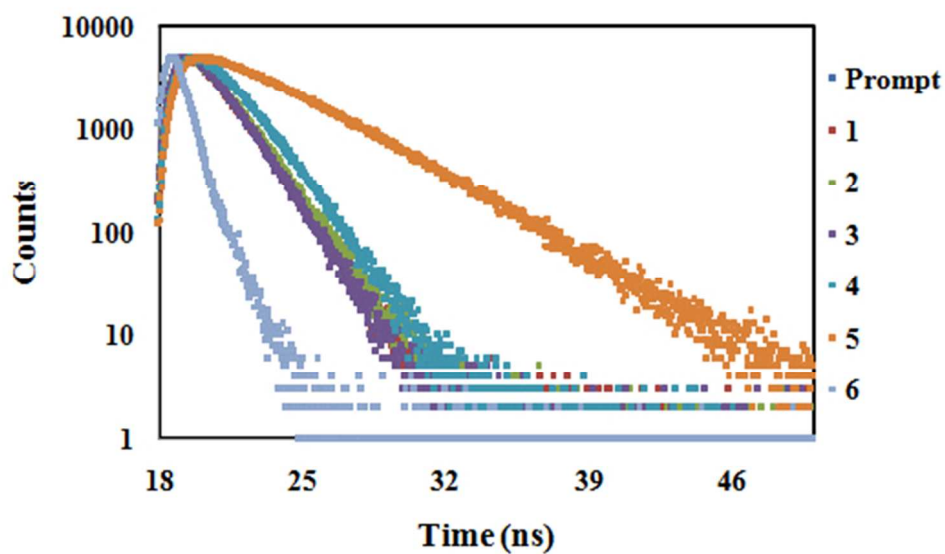


Figure 10

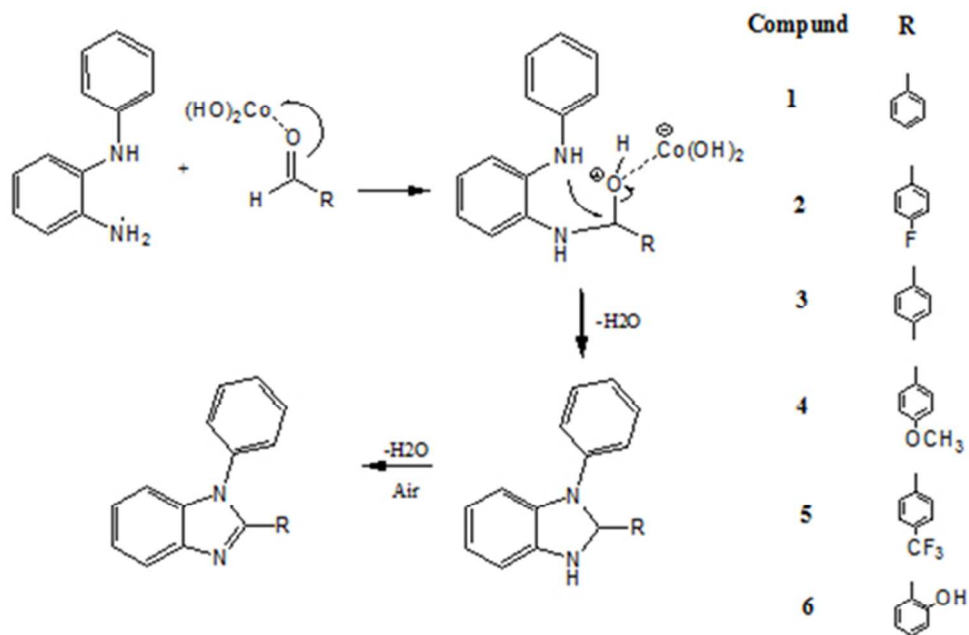
225x168mm (96 x 96 DPI)

**Figure 11**

132x117mm (96 x 96 DPI)

**Figure 12**

144x94mm (96 x 96 DPI)



Scheme 1

157x110mm (96 x 96 DPI)

Table 1 Effect of amount and catalytic activity of catalyst in the synthesis of benzimidazoles (1-6)

S. No	Compound	Time (minutes)	Catalyst (mol %)	yield
1	1	> 500	No entry	trace
2	1	30	10	78
3	1	60	10	89
4	1	60	15	96
5	2	> 500	No entry	trace
6	2	30	10	77
7	2	60	10	86
8	2	60	15	97
9	3	> 500	No entry	trace
10	3	30	10	76
11	3	60	10	87
12	3	60	15	96
13	4	> 500	No entry	trace
14	4	30	10	78
15	4	60	10	87
16	4	60	15	97
17	5	> 500	No entry	trace
18	5	30	10	77
19	5	60	10	87
20	5	60	15	97
21	6	> 500	No entry	trace
22	6	30	10	78
23	6	60	10	86
24	6	60	15	95

Table 2 Fluorescence quantum yield (Φ), lifetime (τ , ns), radiative rate constant (k_r) and nonradiative rate constant (k_{nr}) and dipole moment of benzimidazoles (**1-6**)

Compound	τ (ns)	Φ	k_r (10^8 s^{-1})	k_{nr} (10^8 s^{-1})	μ (D)
1	1.5	0.30	2.06	4.79	3.36 (5.38)
2	1.6	0.52	3.36	3.10	3.02 (6.98)
3	1.4	0.46	3.26	3.83	3.38 (5.68)
4	1.8	0.50	2.72	2.72	2.60 (4.61)
5	4.2	0.53	1.26	1.12	3.43 (7.12)
6	3.3	0.54	1.66	1.41	3.06 (5.26)

values in the parenthesis corresponds to excited state dipole moment

Table 3 Free energy change ($\Delta G_{\text{hex-sol}}$, kcal/mol) and reorganization energies (λ , kcal/mol) of 1-6

Solvents	1		2		3		4		5		6	
	$(\Delta G_{\text{hex-sol}}$	λ										
Hexane	0	4.84	0	5.66	0	5.52	0	3.84	0	5.17	0	8.01
Dioxane	0.2	4.97	0.3	4.87	0.3	6.05	0.36	4.51	0.17	5.45	0.6	8.13
Benzene	0.91	6.41	0.12	6.04	0.12	6.45	0.45	5.36	0.16	6.09	0.8	8.13
Diethylether	1.19	7.02	0.1	6.58	0.1	6.45	0.51	5.60	0.07	6.09	1	8.29
Chloroform	1.5	8.13	0.3	6.94	0.3	7.57	0.8	7.24	0.43	5.97	1.4	11.20
Ethyl acetate	1.5	9.02	1.2	8.18	1.2	8.35	1	7.98	0.32	7.20	1.5	11.14
dichloromethane	1.28	7.94	1.49	8.47	1.49	8.01	1.3	8.48	1.07	8.10	1.56	11.75
Propanol	1.57	9.08	1.32	8.97	1.32	9.19	1.5	8.64	0.86	8.53	1.66	10.32
Acetone	1.23	8.91	1.37	9.19	1.37	9.30	1.8	8.64	0.69	8.53	1.49	10.32
methanol	1.23	8.91	1.64	10.32	1.64	9.19	1.8	8.47	0.53	8.86	1.5	9.74
Acetonitrile	1.33	9.19	1.46	10.14	1.46	10.67	1.9	8.80	0.58	9.08	1.06	11.40
DMSO	1.9	10.02	1.29	10.32	1.29	10.67	1.96	8.97	0.25	9.24	0.8	8.51

Table 4 Adjusted Coefficients ($(v_x)_0$, c_a , c_b and c_c) for the Multilinear Regression Analysis of the Absorption v_{ab} and Fluorescence v_{fl} Wavenumbers and Stokes Shift (Δv_{ss}) of **1-6** with the Solvent Polarity/Polarizability, and the Acid and Base Capacity Using the Taft (π^* , α and β) and the Catalan (SPP^N , SA and SB) Scales.

1	(v_x)	$(v_x)_0 \text{ cm}^{-1}$	(π^*)	c_a	c_b
	λ_{ab}	$(3.39 \pm 0.011) \times 10^4$	$-(0.12 \pm 2.39) \times 10^3$	$(1.72 \pm 7.98) \times 10^3$	$-(0.74 \pm 2.35) \times 10^3$
	λ_{fl}	$(2.94 \pm 0.003) \times 10^4$	$(1.47 \pm 9.79) \times 10^3$	$-(11.89 \pm 32.69) \times 10^3$	$(9.73 \pm 26.01) \times 10^3$
	$\Delta v_{ss} = v_{ab} - v_{fl}$	$(0.45 \pm 0.051) \times 10^4$	$-(1.58 \pm 11.54) \times 10^3$	$(13.61 \pm 38.56) \times 10^3$	$-(10.46 \pm 30.68) \times 10^3$
	(v_x)	$(v_x)_0 \text{ cm}^{-1}$	c_{SPP^N}	c_{SA}	c_{SB}
	λ_{ab}	$(3.36 \pm 0.031) \times 10^4$	$(4.84 \pm 3.82) \times 10^3$	$(12.38 \pm 10.58) \times 10^3$	$-(10.18 \pm 8.20) \times 10^3$
2	λ_{fl}	$(3.03 \pm 0.120) \times 10^4$	$-(10.81 \pm 14.69) \times 10^3$	$-(2.29 \pm 40.67) \times 10^3$	$(15.78 \pm 30.51) \times 10^3$
	$\Delta v_{ss} = v_{ab} - v_{fl}$	$(0.33 \pm 0.14) \times 10^4$	$(15.65 \pm 17.52) \times 10^3$	$-(34.67 \pm 48.51) \times 10^3$	$(25.97 \pm 37.58) \times 10^3$
	(v_x)	$(v_x)_0 \text{ cm}^{-1}$	(π^*)	c_a	c_b
	λ_{ab}	$(3.439 \pm 0.013) \times 10^4$	$-(1.03 \pm 3.06) \times 10^3$	$(6.56 \pm 10.22) \times 10^3$	$-(5.34 \pm 8.13) \times 10^3$
	λ_{fl}	$(2.94 \pm 0.044) \times 10^4$	$(2.07 \pm 10.10) \times 10^3$	$-(12.73 \pm 33.75) \times 10^3$	$(9.43 \pm 26.85) \times 10^3$
	$\Delta v_{ss} = v_{ab} - v_{fl}$	$(4.54 \pm 0.055) \times 10^4$	$-(3.09 \pm 12.56) \times 10^3$	$(19.30 \pm 41.97) \times 10^3$	$-(14.77 \pm 33.40) \times 10^3$
3	(v_x)	$(v_x)_0 \text{ cm}^{-1}$	c_{SPP^N}	c_{SA}	c_{SB}
	λ_{ab}	$(3.37 \pm 0.043) \times 10^4$	$(2.67 \pm 5.25) \times 10^3$	$(4.16 \pm 14.53) \times 10^3$	$-(2.49 \pm 11.26) \times 10^3$
	λ_{fl}	$(3.09 \pm 0.120) \times 10^4$	$-(19.13 \pm 14.87) \times 10^3$	$-(46.54 \pm 41.19) \times 10^3$	$(35.10 \pm 31.91) \times 10^3$
	$\Delta v_{ss} = v_{ab} - v_{fl}$	$(0.29 \pm 0.160) \times 10^4$	$(21.70 \pm 19.33) \times 10^3$	$-(59.70 \pm 53.52) \times 10^3$	$(37.59 \pm 41.47) \times 10^3$
	(v_x)	$(v_x)_0 \text{ cm}^{-1}$	(π^*)	c_a	c_b
	λ_{ab}	$(3.57 \pm 0.024) \times 10^4$	$(1.05 \pm 5.39) \times 10^3$	$(0.29 \pm 18.02) \times 10^3$	$(16.98 \pm 25.82) \times 10^3$
3	λ_{fl}	$(2.90 \pm 0.029) \times 10^4$	$-(3.67 \pm 6.64) \times 10^3$	$(8.18 \pm 22.20) \times 10^3$	$(12.61 \pm 40.00) \times 10^3$
	$\Delta v_{ss} = v_{ab} - v_{fl}$	$(0.47 \pm 0.049) \times 10^4$	$(4.72 \pm 11.28) \times 10^3$	$-(7.89 \pm 37.70) \times 10^3$	$(4.37 \pm 60.02) \times 10^3$
	(v_x)	$(v_x)_0 \text{ cm}^{-1}$	c_{SPP^N}	c_{SA}	c_{SB}
	λ_{ab}	$(3.31 \pm 0.066) \times 10^4$	$(8.29 \pm 8.20) \times 10^3$	$-(20.13 \pm 22.70) \times 10^3$	$(14.01 \pm 17.59) \times 10^3$
	λ_{fl}	$(3.00 \pm 0.079) \times 10^4$	$-(14.48 \pm 9.72) \times 10^3$	$(36.19 \pm 26.93) \times 10^3$	$-(28.03 \pm 20.86) \times 10^3$
	$\Delta v_{ss} = v_{ab} - v_{fl}$	$(0.30 \pm 0.137) \times 10^4$	$(23.37 \pm 16.91) \times 10^3$	$-(56.32 \pm 46.83) \times 10^3$	$(42.04 \pm 362.70) \times 10^3$

4	(ν_x)	$(\nu_x)_0 \text{ cm}^{-1}$	(π^*)	c_α	c_β
	λ_{ab}	$(3.33 \pm 0.014) \times 10^4$	$-(0.82 \pm 3.12) \times 10^3$	$(4.92 \pm 10.42) \times 10^3$	$-(3.87 \pm 8.29) \times 10^3$
	λ_{fl}	$(2.92 \pm 0.046) \times 10^4$	$-(1.26 \pm 10.49) \times 10^3$	$-(1.18 \pm 35.05) \times 10^3$	$(0.39 \pm 27.89) \times 10^3$
	$\Delta\nu_{ss} = \nu_{ab} - \nu_{fl}$	$(0.41 \pm 0.059) \times 10^4$	$(0.44 \pm 13.44) \times 10^3$	$(6.09 \pm 44.90) \times 10^3$	$-(4.26 \pm 35.73) \times 10^3$
5	(ν_x)	$(\nu_x)_0 \text{ cm}^{-1}$	c_{SPP}^N	c_{SA}	c_{SB}
	λ_{ab}	$(3.32 \pm 0.010) \times 10^4$	$(10.63 \pm 4.21) \times 10^3$	$(40.85 \pm 18.63) \times 10^3$	$-(40.65 \pm 20.34) \times 10^3$
	λ_{fl}	$(2.92 \pm 0.033) \times 10^4$	$-(33.04 \pm 13.67) \times 10^3$	$-(119.42 \pm 60.55) \times 10^3$	$(113.09 \pm 66.08) \times 10^3$
	$\Delta\nu_{ss} = \nu_{ab} - \nu_{fl}$	$(0.40 \pm 0.042) \times 10^4$	$(43.67 \pm 17.56) \times 10^3$	$-(160.27 \pm 777.72) \times 10^3$	$(153.74 \pm 84.87) \times 10^3$
6	(ν_x)	$(\nu_x)_0 \text{ cm}^{-1}$	(π^*)	c_α	c_β
	λ_{ab}	$(3.33 \pm 0.011) \times 10^4$	$-(0.38 \pm 2.47) \times 10^3$	$(3.52 \pm 8.26) \times 10^3$	$-(2.77 \pm 6.57) \times 10^3$
	λ_{fl}	$(2.90 \pm 0.033) \times 10^4$	$-(0.76 \pm 7.56) \times 10^3$	$-(1.99 \pm 25.26) \times 10^3$	$(1.08 \pm 20.10) \times 10^3$
	$\Delta\nu_{ss} = \nu_{ab} - \nu_{fl}$	$(0.43 \pm 0.043) \times 10^4$	$(0.38 \pm 9.76) \times 10^3$	$(5.51 \pm 32.60) \times 10^3$	$-(3.85 \pm 25.94) \times 10^3$
6	(ν_x)	$(\nu_x)_0 \text{ cm}^{-1}$	c_{SPP}^N	c_{SA}	c_{SB}
	λ_{ab}	$(3.33 \pm 0.009) \times 10^4$	$(8.85 \pm 8.58) \times 10^3$	$(34.33 \pm 15.84) \times 10^3$	$-(35.00 \pm 17.29) \times 10^3$
	λ_{fl}	$(2.89 \pm 0.026) \times 10^4$	$-(21.60 \pm 10.92) \times 10^3$	$-(76.20 \pm 48.34) \times 10^3$	$-(72.27 \pm 52.76) \times 10^3$
	$\Delta\nu_{ss} = \nu_{ab} - \nu_{fl}$	$(0.44 \pm 0.034) \times 10^4$	$(30.45 \pm 14.08) \times 10^3$	$-(110.53 \pm 62.36) \times 10^3$	$(107.27 \pm 68.05) \times 10^3$
6	(ν_x)	$(\nu_x)_0 \text{ cm}^{-1}$	(π^*)	c_α	c_β
	λ_{ab}	$(3.41 \pm 0.005) \times 10^4$	$(0.11 \pm 1.11) \times 10^3$	$(1.23 \pm 3.70) \times 10^3$	$-(1.20 \pm 2.94) \times 10^3$
	λ_{fl}	$(2.74 \pm 0.049) \times 10^4$	$-(8.30 \pm 11.17) \times 10^3$	$(28.15 \pm 37.32) \times 10^3$	$-(21.86 \pm 29.70) \times 10^3$
	$\Delta\nu_{ss} = \nu_{ab} - \nu_{fl}$	$(0.66 \pm 0.052) \times 10^4$	$(8.41 \pm 11.82) \times 10^3$	$-(26.91 \pm 39.48) \times 10^3$	$(20.66 \pm 31.42) \times 10^3$
6	(ν_x)	$(\nu_x)_0 \text{ cm}^{-1}$	c_{SPP}^N	c_{SA}	c_{SB}
	λ_{ab}	$(3.41 \pm 0.005) \times 10^4$	$(3.12 \pm 2.06) \times 10^3$	$(11.81 \pm 9.13) \times 10^3$	$-(12.16 \pm 9.97) \times 10^3$
	λ_{fl}	$(2.78 \pm 0.038) \times 10^4$	$-(21.59 \pm 15.79) \times 10^3$	$(81.86 \pm 69.89) \times 10^3$	$-(77.27 \pm 76.28) \times 10^3$
	$\Delta\nu_{ss} = \nu_{ab} - \nu_{fl}$	$(0.63 \pm 0.040) \times 10^4$	$(24.71 \pm 16.21) \times 10^3$	$-(93.68 \pm 71.79) \times 10^3$	$(89.43 \pm 78.34) \times 10^3$

Table 5 Slopes and intercepts of the solvatochromic plots of the CT Fluorescence of the benzimidazoles (1-6)

Compound	Nonpolar solvents and Polar solvents		Polar solvents		Nonpolar solvents and Polar solvents	
	$hc\Delta_{\text{abs}}^{\text{vac}}$, eV	$\mu_e (\mu_e - \mu_g) / a_0^3$	$hc\Delta_{\text{abs}}^{\text{vac}}$, eV	$\mu_e (\mu_e - \mu_g) / a_0^3$	$\mu_e (\mu_e - \mu_g) / a_0^3$ eV	μ , D
1	3.82	0.97	3.92	1.22	1.407	12.41
2	3.86	1.09	3.96	1.15	1.509	13.08
3	3.73	0.74	3.92	1.02	1.115	13.20
4	3.83	1.08	3.95	1.21	1.358	12.83
5	3.74	1.16	3.85	1.30	1.362	13.32
6	3.56	0.98	3.62	1.25	1.023	10.84

Table 6 Electron density (e.u) of azomethine nitrogen (3) and oxygen (26) of **6**.

Atom	II	II*	III
Azomethine nitrogen(3)	-0.395	-0.455	0.313
Oxygen(26)	-0.570	-0.528	-0.697

*corresponds to excited state